J. Eur. Opt. Society-Rapid Publ. 2025, **21**, 14

https://doi.org/10.1051/jeos/2025010
Available online at: https://jeos.edpsciences.org

EOSAM 2024
Guest editors: Luca De Stefano and Raffaele Velotta

Journal of the European Optical Society-Rapid Publications

RESEARCH ARTICLE OPEN ACCESS

Type-I intermittency route to the chaos in passively Q-switched Tm:YLF laser emitting at 2.3 µm

Matthieu Glasset, Hippolyte Dupont, Patrick Georges, and Frédéric Druon*

Université Paris-Saclay, Institut d'Optique Graduate School, CNRS, Laboratoire Charles Fabry, 91127 Palaiseau, France

Received 31 December 2024 / Accepted 26 February 2025

Abstract. We report on an original chaotic dynamic behavior of a Tm-doped Q-switched laser operating on the $^3H_4 \rightarrow {}^3H_5$ transition emitting at 2.3 µm using a Tm:YLF crystal, with optional co-lasing at 1.9 µm via the $^3F_4 \rightarrow {}^3H_4$ transition. This study specifically investigates the chaotic and intermittent dynamics originally observed in this laser. Experimental observations reveal an atypical type-I intermittency route to chaos, linked to cascade transitions and characterized using Poincaré maps, entropy calculations, and phase-space reconstructions. The analysis highlights synchronization losses between the Q-switched pulse train and relaxation oscillations in the 1.9 µm cascade laser as a driver of chaotic instabilities. These findings deepen the understanding of chaotic regimes in Tm-doped lasers and provide insights for optimizing the stability of MIR laser systems for advanced photonic applications. Further modeling is needed to fully elucidate the interplay of dual-wavelength dynamics and the observed chaotic behavior.

Keywords: Solid state laser, MIR laser, Tm-doped laser, Q-switch laser.

1 Introduction

The advancement of Q-switched lasers operating in the short-wave infrared (SWIR) to mid-infrared (MIR) spectrum represents a significant and promising area of research, with specific applications including atmospheric gas sensing, non-invasive blood glucose monitoring, and the pumping of mid-infrared optical parametric oscillators utilizing non-oxide nonlinear crystals. Of particular interest are wavelengths around 2.3 µm, which are well-suited to these applications. Trivalent thulium ions (Tm^{3+}) possess an energy level structure that supports emission at around 1.9 µm via the $^3F_4 \rightarrow {}^3H_6$ transition, as well as at 2.3 µm via the $^3H_4 \rightarrow {}^3H_5$ transition. Extensive research has been conducted on Tm-doped materials under Q-switching regimes [1–5], with observations of chaotic behavior, particularly at 2.3 µm [6–9]. However, this sensitivity to instability and chaotic regimes has not yet been systematically analyzed. The study of chaotic dynamics for such lasers holds great interest as it depends on our understanding of laser stability issues. Indeed, Tm-doped lasers operating above 2 µm have in this matter a strong propension to reach chaotic regimes, since such materials often involve cascade energetic transitions. The $^3H_4 \rightarrow {}^3H_5$ laser transition at 2.3 µm (wavelength of interest here) is actually linked to the $^3F_4 \rightarrow {}^3H_6$ transition emitting at 1.9 µm via the long (e.g. 11 ms in Tm:YLF) intermediate metastable level: $^3F_4$, cf. Figure 1a.

Interestingly, Q-switched Tm-doped lasers exhibit an unique intermittency route to chaos, an unusual behavior for Q-switched lasers, such as those that are doped with Nd for example. This atypical chaotic behavior with intermittency appears inherently linked to the cascade transitions within the laser, as described by De Valcárcel et al. [10]. Although intermittency routes to chaos have been documented in other laser systems, often induced through external coupling [11–16] or in multiple-cavity Q-switched systems [17], such behavior has not, to our knowledge, been previously reported in passively Q-switched systems.

We demonstrate here that a type-I intermittency route to chaos can be observed within a single Q-switched cavity, which is a very atypical route for passively Q-switching.

2 Experimental results

To make a detailed examination of the dynamic behavior of a Tm:YLF laser operating on the $^3H_4 \rightarrow {}^3H_5$ transition, emission at 2.3 µm alone or in cascade co-laser operation (2.3 µm and 1.9 µm) have been studied. For this, as shown in Figure 1b, a Q-switched cavity operating at 2.3 µm using a Cr:ZnSe saturable absorber crystal is performed. An optional "cw" cavity emitting at 1.9 µm sharing the Tm:YLF gain crystal is also implemented to test the behavior

* Corresponding author: frederic.druon@institutoptique.fr

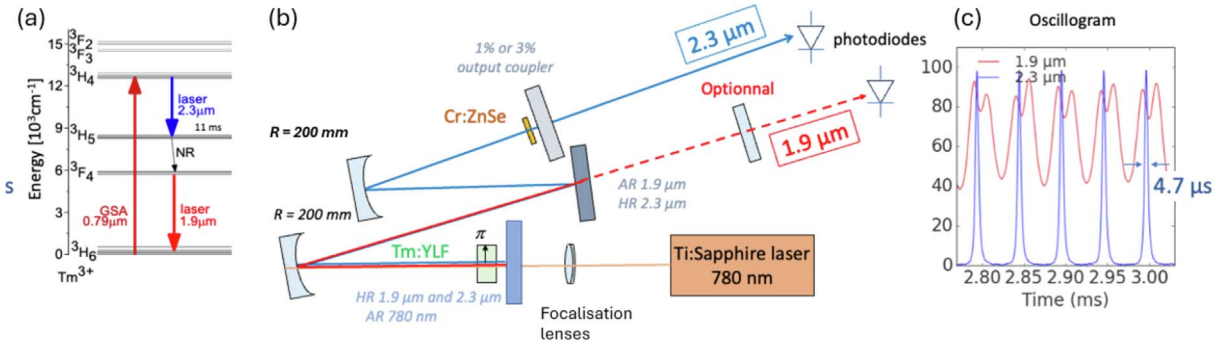

Fig. 1. (a) Experimental setup allowing co-lasing at 1.9 µm and 2.3 µm. The saturable absorber is placed in the 2.3 µm laser cavity exclusively. (b) Normalized impulsion train at 2.3 µm and laser intensity at 1.9 µm for a stable Q-switch. (c) Energy levels of Tm^{3+}. GSA: Ground State Absorption, NR: Non Radiative transition.

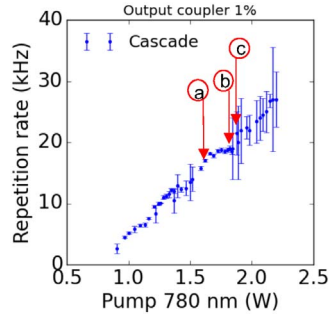

Fig. 2. Dependence of the pulse repetition rate on the pump power at 780 nm indicating the points where the oscillograms (a)–(c) from the Figure 3 have been taken. The laser emission at 1.9 µm is not permitted in this case.

with and without cascade laser. In these configurations, Q-switched regime is obtained between 1 and 30 kHz with a constant pulse duration of 4.7 µs (Fig 1c). The repetition rate of the Q-switching increases, as expected, linearly versus the pump power (Fig. 2). The error bars indicate the root mean square (rms) value of the repetition rate measurements. In both cases (with or without cascade laser), chaotic zones can be clearly identified when the dispersion of the repetition rate explodes [18]. On the opposite, stable zone occurs with relatively low dispersion in the repetition rates. Different typical regimes exploring the route to chaos has been further analysed (shown in Figs. 2 and 3). These different setting points are the stable regime (a), the chaotic regime (c) and the intermittency regime (b) in between.

We will focus now on the transition regime from stable Q-switching to chaotic regime around 20 kHz. To analyse the different regimes, we plot in Figure 3 the oscillograms (first line). Further analysis is possible extracting from these oscillograms the pulse peak powers which allows to have access to key parameters for chaos study, such as sample entropy and Poincaré map (Fig. 3 second line) [19, 20]. Another parameter useful to quantify the route to chaos is the entropy. The corresponding histograms are given in Figure 3 third line. The entropy of the peaks is evaluated using the function "sampen" from the "nolds" Python library. The parameters are the following: the embedded dimension is $m = 4$, and the tolerance is 2%. The experiment then shows an increase, with the selected parameters, of this entropy from 0 when stable up to 1.55 in the chaotic regime. The results showed in Figure 3 will be more discussed in the later part of the article.

3 Discussion and interpretation

Let us focus on the intermittency regime. In this region the entropy is around 0.55; an intermediate value due to the observation of laminar phases [19, 20] closed to a stable regime interrupted by stochastic intermittencies. One can then isolate the laminar phases in the Poincaré diagram which consists in plotting the peak powers versus their antecedent: $I_{n+1} = f(I_n)$. During the laminar phase, the points are above the bisector line. In the case of type I intermittency scenario, these laminar phase points can be fitted by a polynomic (typically cubic). This fit is plotted in orange in the Poincaré map, column b in Figure 3. Moreover, one can observe, still in the type-I intermittency scenario accordance, that this fitting curve approaches the bisector line around the point (1, 1). To perform this analysis, we select another dataset in the same configuration with six laminar phases with high regularity in the laminar length (between 7 and 8); this dataset point is plot in Figure 4b. The minimum distance (ε) between the fitting curve and the bisector line is then related to the laminar length (L): $L = \varepsilon^{-\lambda}$ with $\lambda = 0.5$ within the theory of the type-I intermittency scenario. In our case $e = 0.0165$ and the mean value of $L = 7.75$, this leads to $\lambda = 0.499$ corroborating the type I intermittency scenario.

Using this fit it is then possible to simulate the theoretical evolution of the peak power. As shown in Figure 4a, even if the theoretical curve can be extended beyond the (1, 1) point, the real peak power is confined inside the Poincare map, which extends over the square with side 1. Then, when $I_{n+1} = f(I_n) > 1$, the peak power is folded under the bissector line. The folding process respects the Baker transformation which consists of a two steps transformation:

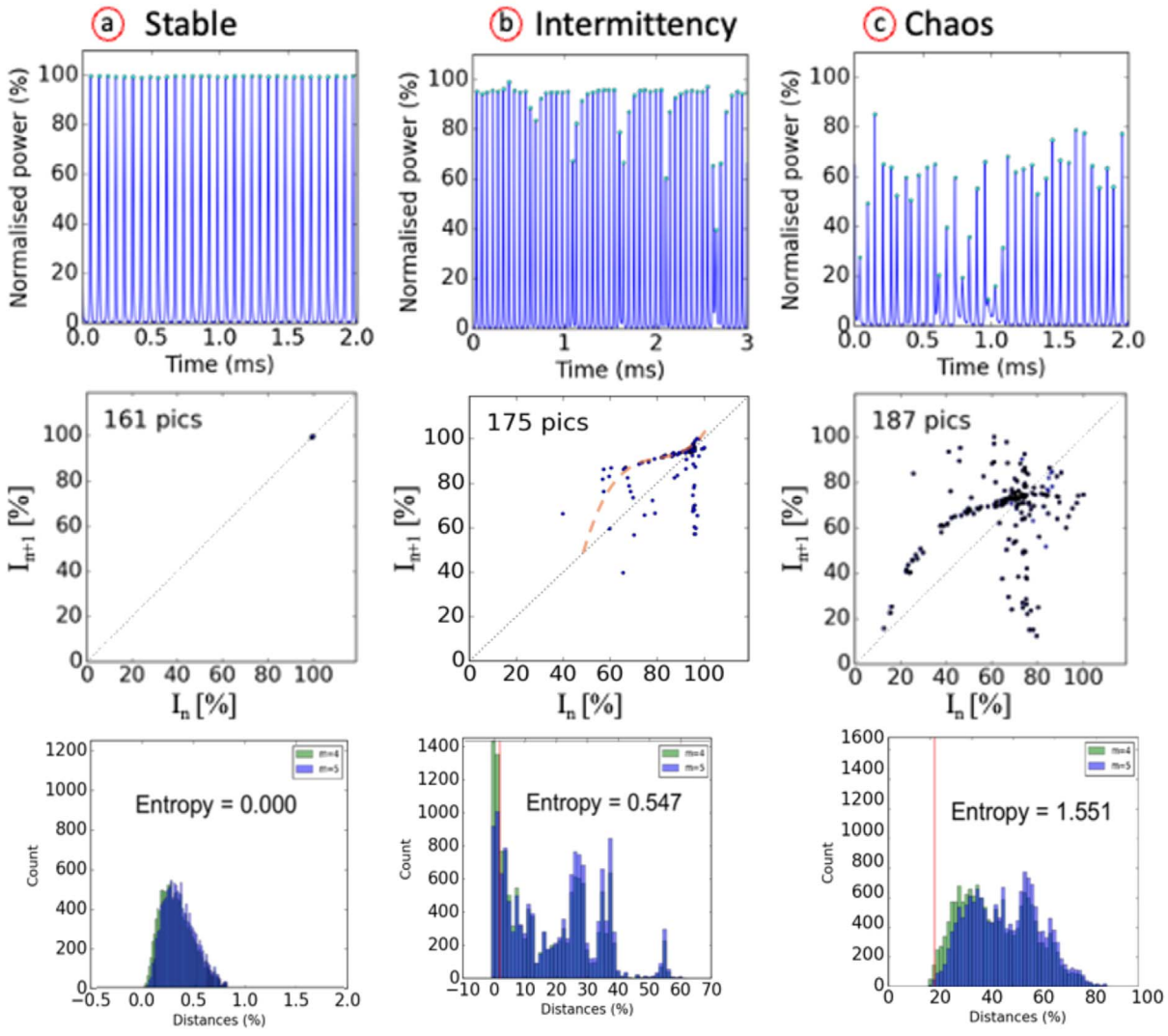

Fig. 3. The first line shows the oscillograms, the second line presents the corresponding Poincaré maps of the peak intensities of Q-switched pulses $I_{n+1} = f(I_n)$, and the third line presents histograms used for calculating the peak entropy (embedded dimension $m = 4$ and 5). Tree different operation regimes are presented: 1st column (a) corresponds to a stable Q-switched regime, 2nd column: (b) corresponds to an intermittency regime, 3th column (c) corresponds to a chaotic regime.

- First, the part of the theoretical curve outside the map is contracted over the x-axis and stretched over the y-axis. The contracting and stretching coefficients are difficult to calculate and we obtained estimations from the experimental data.
- Second, the obtained modified curve is then folded under the bisector line. The expected peak power is then under the bisector line which explains the characteristic "drop" of the intermittence.

Figure 4b, shows the experiment points and the theoretical points for two consecutive laminar phases. To consider theoretically the intermittency, a baker transformation has to be introduced. We consider that, if the normalized I_{n+1} is above 1, then the intermittency occurs and the next point is found using the baker transformation on the folded and stretched part of the fitting curve. Since the normalization is not obvious, one must consider the experimental data. One important point to consider here concerns the start and the end of the laminar phase to appropriately evaluate, first, its length and second, concerning the baker's transformation, to also have a good estimation of when to cut the fitting curve before the stretching and the folding of the dough. In our case, since the intermittency occurs quickly after the minimum distance, the baker's transformation involves a large stretching of the dough in the vertical direction [21] before being folded under the bisector line. The contraction ratio ([20], p, 254) is around $\beta = 0.03$ which implies a folding of the "fitting curve" almost linear and quasi vertical. In Figure 4b, we found a good accuracy for a very strong asymmetric stretching of the dough considering the first points of the intermittencies.

Observing the Poincaré maps, one can notice that the density of points is more important when the laminar phase

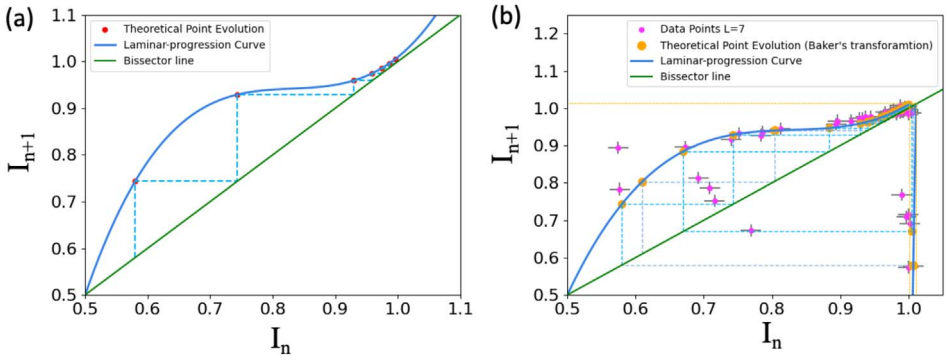

Fig. 4. Poincaré maps representing the laminar phase evolution $I_{n+1} = f(I_n)$: (a) theoretical evolution of a single laminar phase with $L = 7$; (b) theoretical points of three successive $L = 7$ laminar phases considering relaminarization using the baker's transformation. The relaminarization process consists of cutting the blue curve $f(x)$, taking the upper part, stretching it and folding it back: explaining then the differences between (a) and (b). Experimental points for six consecutive cycles of $L = 7$–8 laminar phases are plotted for comparison.

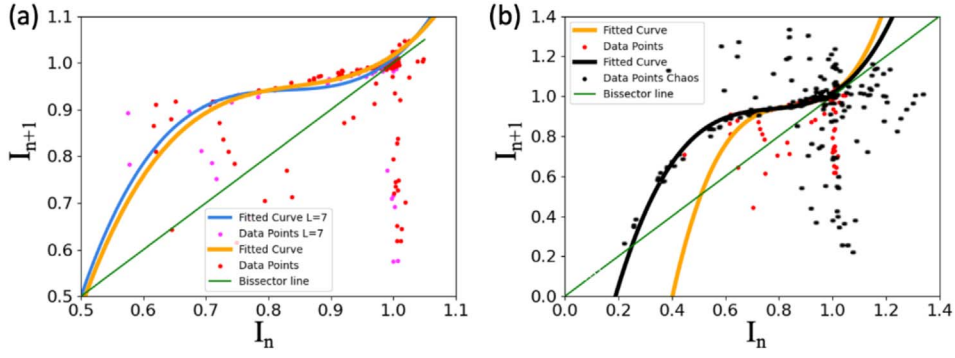

Fig. 5. Poincaré maps representing the laminar phase evolution $I_{n+1} = f(I_n)$: (a) comparison between two different data acquisitions: six consecutive laminar phases counting around seven peaks each : experimental points in purple with the fit in orange and 16 laminar phases : experimental points in red with the fit in blue; (b) a comparison between the intermittency (red points) and chaotic regime (black points); fits are represented, fixing (*black*) or not (*orange*) the intersection value with the bisector line.

approaches the bisector. This corresponds to the region where the laminar phase has its minimum variation and where the standard deviation of the measurements is in the same order of magnitude of this variation. It seems important in our method to have a consequent number of laminar phases to reduce the incertitude on the ε factor. Indeed, since ε is comparable to typical standard deviations of the measured peak intensities, the accuracy of ε is interesting to consider. With a standard deviation of 1.5% and in the case of six laminar phase measurements, the precision is about 0.0061 and it drops to 0.0037 in the case of 16 laminar phases. According to these considerations, we compare the results of the two datasets we studied: (i) the case of 6 very regular laminar phases and (ii) the case of 16 laminar phases with stronger dispersion in their length. Representing these two sets of data, we observed similar evolution, Figure 5a with comparable fitting curves. One last question interesting to consider appears when observing the Poincaré map representation of the chaotic regime still very similar to the intermittency ones, see Figure 5b, where the points for the chaotic regime are in black. Indeed, we observe a kind of extension of the cubic shape tendency to lower values with a crossing with the bisector. Since the intermittency regime does not reach these relatively low values of relative peak intensity, the fitting curve crosses the bisector around 0.5 whereas that for the chaotic regime has this crossing around 0.2. To go further and to evaluate a potential error in the fitting process, we fitted the intermittency regime but forcing the intersection value with the bisector line at the point (0.2, 0.2). The fit in this last case is represented in black in Figure 5b (and in Fig. 3) and gives $\varepsilon = 0.0168$ and $\lambda = 0.501$ which is very similar to the previous case and shows that points lying far from the accumulation are underestimated in the fitting process but does not impact strongly the ε value.

The Poincaré map offers an interesting and simple tool to discriminate the laser dynamics. By examining the structure of the trajectory in a 2D plane, we were able to quantify the stability of the pulse train and characterize the nature of the intermittencies. However, the laser under consideration has many dynamic variables. This diversity of physical quantities cannot be fully measured experimentally, which prevents us from studying the entire trajectory of the system in its phase space. In addition, our simulations

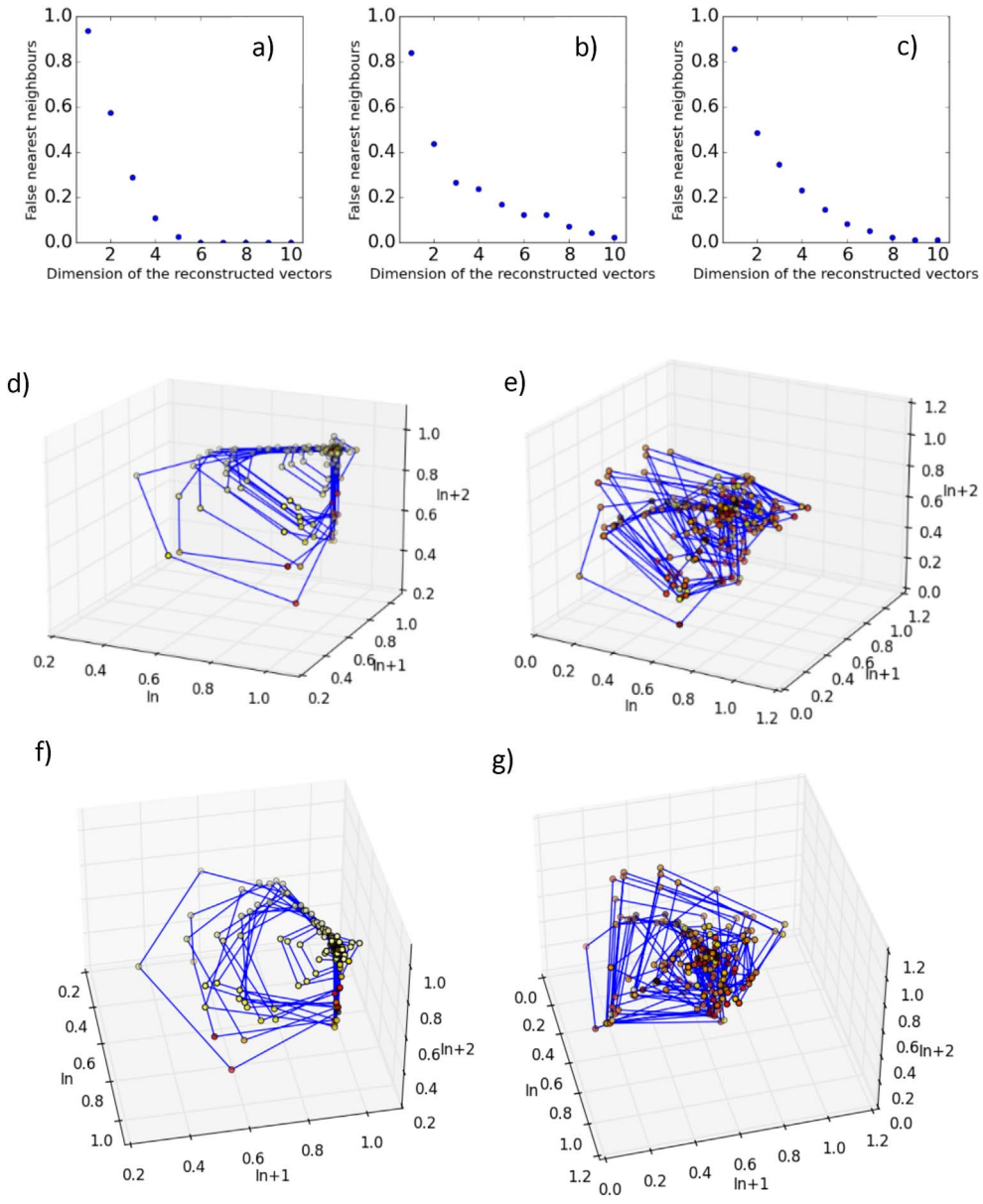

Fig. 6. First line: Proportion of false nearest neighbours versus the dimension of the reconstructed vectors in the case (a) stable (b) intermittences, and (c) chaotic. Second and Third lines: 4D projection of the reconstructed phase space for (d) and (f) intermittent regime and (e) and (g) chaotic regime.

of the rate equations do not, for the moment, provide results like those obtained experimentally, perhaps indicating the need to take into account variables whose impact on dynamics is not yet understood. Hence, to explore more deeply the system dynamics, we realised a phase space reconstruction using a model based on Taken's theorem [22]. To do so, we construct the vectors $Y[n]$ such as:

$$Y[\,n] = \{I[n], I[n + \tau f_e], \ldots, I[n + (d_e - 1)\tau f_e]\}$$

where $I[n]$ represents the n-th measured point of the output intensity at 2.3 µm, τ is the time lag, f_e is the sampling frequency of our scope and d_e is the embedding dimension.

The main difficulty of this reconstruction lies on the choice of the embedding dimension and the right time lag to ensure that the trajectory unfolding is complete. For the time lag, we have to consider a sufficiently long time to ensure the independence of the variables used to reconstruct the system's phase space. But, since the system is chaotic, the exponential growth of small perturbations, obliges us to have a sufficiently short time lag to ensure connection between the variables ([23], p. 25). Hence, we chose as our time lag, the natural emission time of laser impulsions, by working directly with the maximal intensities extracted from the time track. Here, we consider that the repetition rate is sufficiently long to let the system explore

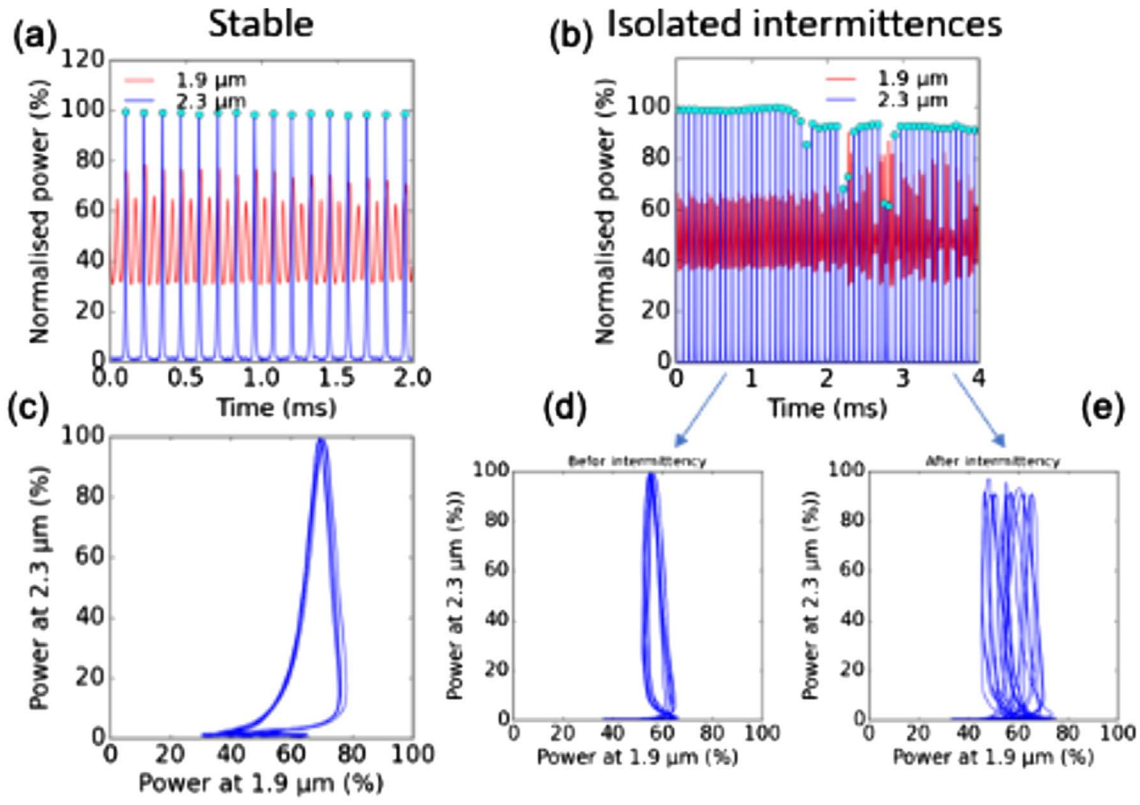

Fig. 7. Simultaneous, dual monitoring of the cascade laser: 2.3-µm Q-switch laser (*blue*) and 1.9-µm laser (*red*). First line: oscillograms. Second line: 2.3 µm laser power versus 1.9 µm laser power.

his phase space trajectory. This allows to get "independent variables" and since the build-up time of the pulse is linked to the precedent pulse, we keep a correlation between $I[n]$ and $I[n + \tau f_e]$. Choosing the dimension of the $Y[n]$ vectors is less trivial. However, Kennel et al. [24] have proposed to evaluate the proportion of false nearest neighbours in the trajectory.

Figure 6 shows the reconstruction for the intermittent and chaotic regimes presented in Figure 3. We observe an embedding dimension of our system between 6 and 10, depending on the dynamics adopted by the laser. From our study, we can deduce ([23], p. 46) an upper bound for the attractor dimension of our system: $d_A \leq \frac{d_e}{2} \leq 5$, where d_A is the attractor dimension and d_e is the embedding dimension.

In our case, we are able to observe simultaneously both laser emissions at 2.3 µm and 1.9 µm giving us the opportunity to access another projection of the phase space. Indeed, it is interesting to look at the 1.9 µm laser relaxation operation after the 2.3 µm Q-switch pulse to observe whether the $^3F_4$ population oscillates synchronously with the Q-switch tempo. For example, the first column of Figure 7a represent stable train where both 2.3 µm Q-switched pulses and 1.9 µm relaxation are synchronized. Plotting (Fig. 7c) the phase diagram $I_{2.3\ \mu m}$ versus $I_{1.9\ \mu m}$ then leads to a well-defined cycle. To evaluate the intermittency regime in comparison, we study the particular interesting case where intermittencies occur after a stable regime (Fig. 7b). In this case it is interesting to observe the synchronization before and during the inherencies. Indeed, whereas in the stable regime the cycling regime (Fig. 7d) indicates a good synchronization, as soon as the intermittencies occur this synchronization is lost and the relaxation oscillations of the 1.9 µm laser become erratic (Fig. 7b) leading to absence of stable cycling (Fig. 7e). This study is interesting since it seems to indicate that a hypothesis of a loss of synchronization between the Q-switch laser at 2.3 µm and the population of the $^3F_4$ metastable regime as an aggravating phenomenon to explain the chaotic instabilities seem very probable.

4 Conclusion

In conclusion, this study has provided insights into the dynamic behavior of Q-switched Tm:YLF lasers operating on the $^3H_4 \rightarrow {}^3H_5$ transition at 2.3 µm, particularly focusing on their chaotic and intermittent regimes. The investigation highlights a unique intermittency route to chaos, which is atypical in passively Q-switched lasers and appears to be inherently tied to the cascade energy transitions of trivalent thulium ions. The analysis of stable, intermittent, and

chaotic regimes through experimental tools such as Poincaré maps, entropy calculations, and phase diagrams has demonstrated the complexity of these dynamics. The findings tend to confirm the type-I intermittency scenario in the Q-switching dynamics, with laminar phases preceding chaotic transitions. The study also underscores the critical role of synchronization loss between the Q-switched laser at 2.3 µm and the relaxation oscillations of the 1.9 µm cascade laser in driving chaotic behavior. This desynchronization provides a plausible explanation for the onset of instability and chaotic regimes. These results not only deepen the understanding of chaotic dynamics in Q-switched Tm-doped lasers but also provide a basis for future studies aiming to control or exploit such instabilities in advanced photonic applications, including atmospheric sensing and medical diagnostics. Further exploration and modelization of dual-wavelength interactions and synchronization phenomena will be valuable in advancing the development and stability of mid-infrared laser systems. The current numerical model actually do not totally explain the intensity of the chaotic behavior and extra coupled phenomenon is under investigation. The analysis of intermittent dynamics provides valuable insights into complex systems, contributing to our understanding of the fundamental principles underlying natural and engineered systems such as cascade laser emitting in the MIR. In the context of this study, the fact that Tm-doped systems are prone to intermittency chaotic transitions makes Q-switched lasers using this crystal an interesting subject of investigation. These discoveries enhance our understanding of the intricate dynamics of Tm-doped lasers, impacting the design and optimization of MIR-range lasers for diverse applications, with potential extensions to other cascade lasers.

Funding

Agence Nationale de la Recherche (ANR): projects PULSE ANR-20-CE30-0026 and SPLENDID2 ANR-19-CE08-0028.

Conflicts of interest

The authors declare that they have no competing interests to report.

Data availability statement

Data underlying the results presented in this paper are not publicly available at this time but may be obtained from the authors upon reasonable request.

Author contribution statement

Conceptualization F.D., M.G., and H.D.; Methodology, F.D., M.G., and H.D.; Software, M.G., H.D. and F.D.; Validation, F.D., M.G., and H.D.; Formal Analysis, F.D., M.G. and H.D; Investigation, F.D., M.G., and H.D; Resources, F.D., and P.G; Data Curation, F.D., M.G., H.D and P.G; Writing – Original Draft Preparation, M.G. and F.D.; Writing – Review & Editing, F.D., M.G., H.D and P.G; Visualization, F.D., M.G., H.D and P.G.; Supervision, F.D and P.G.; Project Administration, F.D.; Funding Acquisition, F.D. and P.G

References

1 Faoro R, Kadankov M, Parisi D, Veronesi S, Tonelli M, Petrov V, Griebner U, Segura M, Mateos X, Passively Q-switched Tm:YLF laser, *Opt. Lett.* **37**, 1517 (2012). https://doi.org/10.1364/OL.37.001517.

2 Yao B, Tian Y, Li G, Wang Y, InGaAs/GaAs saturable absorber for diode-pumped passively Q-switched dual-wavelength Tm:YAP lasers, *Opt. Express* **18**, 13574 (2010). https://doi.org/10.1364/OE.18.013574

3 Du Y, Yao B, Duan X, Cui Z, Ding Y, Ju Y, Shen Z, Cr:ZnS saturable absorber passively Q-switched Tm, Ho:GdVO4 laser, *Opt. Express* **21**, 26506 (2013). https://doi.org/10.1364/OE.21.026506.

4 Segura M, Kadankov M, Mateos X, Pujol MC, Carvajal JJ, Aguiló M, Díaz F, Griebner U, Petrov V, Passive Q-switching of the diode pumped Tm^{3+}:$KLu(WO_4)_2$ laser near 2-µm with Cr^{2+}:ZnS saturable absorbers, *Opt. Express* **20**, 3394 (2012). https://doi.org/10.1364/OE.20.003394.

5 Canbaz F, Yorulmaz I, Sennaroglu A, 2.3-µm Tm^{3+}:YLF laser passively Q-switched with a Cr^{2+}:ZnSe saturable absorber, *Opt. Lett.* **42**, 1656 (2017). https://doi.org/10.1364/OL.42.001656.

6 Wang S, Huang H, Chen H, Liu X, Liu S, Xu J, Shen D, High efficiency nanosecond passively Q-switched 2.3 µm Tm:YLF laser using a $ReSe_2$-based saturable output coupler, *OSA Continuum* **2**, 1676 (2019). https://doi.org/10.1364/OSAC.2.001676.

7 Huang H, Wang S, Chen H, Antipov OL, Balabanov SS, Shen D, High power simultaneous dual-wavelength CW and passively-Q-switched laser operation of LD pumped Tm:YLF at 1.9 and 2.3 µm, *Opt. Express* **27**, 38593 (2019). https://doi.org/10.1364/OE.381821.

8 Zhang H, He J, Wang Z, Hou J, Zhang B, Zhao R, Han K, Yang K, Nie H, Sun X, Dual-wavelength, passively Q-switched Tm:YAP laser with black phosphorus saturable absorber, *Opt. Mater. Express* **6**, 2328 (2016). https://doi.org/10.1364/OME.6.002328.

9 Kifle E, Loiko P, Guillemot L, Doualan J-L, Starecki F, Braud A, Hideur A, Camy P, Design and modeling of a passively Q-switched diode-pumped Thulium laser at 2.3 µm, *Opt. Commun.* **500**, 127219 (2021). https://doi.org/10.1016/j.optcom.2021.127219.

10 De Valcárcel GJ, Roldán E, Espinosa V, Vilaseca R, Types I and II intermittencies in a cascade model (Physics Letters A 206 (1995) 359), *Phys. Lett. A* **209**, 388 (1995). https://doi.org/10.1016/0375-9601(95)00628-G.

11 Kim C-M, Lee K-S, Kim JM, Kwon S-O, Kim C-J, Lee J-M, Route to chaos through the type I intermittency of a gain-modulated CO_2 laser caused by the discharge instability at low frequency, *J. Opt. Soc. Am.* **10**, 1651 (1993). https://doi.org/10.1364/JOSAB.10.001651.

12 Villafana-Rauda E, Chiu R, Mora-Gonzalez M, Casillas-Rodriguez F, Medel-Ruiz CI, Sevilla-Escoboza R, Dynamics of a Q-switched Nd:YVO4/Cr:YAG laser under periodic modulation, *Results Phys.* **12**, 908 (2019). https://doi.org/10.1016/j.rinp.2018.12.050.

13 Martel G, Bennoud M, Ortac B, Chartier T, Nunzi JM, Boudebs G, Sanchez F, Dynamics of a vectorial neodymium-doped fibre laser passively *Q* switched by a polymer-based saturable absorber, *J. Mod. Opt.* **51**, 85 (2004). https://doi.org/10.1080/09500340408234594.

14 Letellier C, Bennoud M, Martel G, Intermittency and period-doubling cascade on tori in a bimode laser model. *Chaos Solitons Fractals* **33**, 782 (2007). https://doi.org/10.1016/j.chaos.2006.01.109.
15 Mgharaz D, Brunel M, Chaotic regimes and synchronization in Tm^{3+}-doped fiber laser with pump modulation, *J. Opt. Soc. Am. B* **36**, 2184 (2019). https://doi.org/10.1364/JOSAB.36.002184.
16 Kim GU, Choo HT, Kim DI, Park Y-J, Gong S-H, Kim C-M, Transition through on–off intermittency in Nd: YAG laser systems pumped by laser diodes, *J. Opt. Soc. Am. B* **20**, 302 (2003). https://doi.org/10.1364/JOSAB.20.000302.
17 Huang HT, et al. Intermittent oscillation of 1064 nm and 1342 nm obtained in a diode-pumped doubly passively Q-switched Nd:YVO_4 laser, *Appl. Phys. B* **96**, 815 (2009). https://doi.org/10.1007/s00340-009-3586-9.
18 Kovalsky M, Hnilo A, Chaos in the pulse spacing of passive *Q*-switched all-solid-state lasers, *Opt. Lett.* **35**, 3498 (2010). https://doi.org/10.1364/OL.35.003498.
19 Pomeau Y, Manneville P, Intermittent transition to turbulence in dissipative dynamical systems, *Commun. Math. Phys.* **74**, 189 (1980). https://doi.org/10.1007/BF01197757.
20 Bergé P, Pomeau Y, Vidal Ch, *L'ordre dans le chaos: Vers une approche déterministe de la turbulence* (Hermann Edition, Paris, 1997).
21 Dorfman JR, in *An introduction to chaos in nonequilibrium statistical mechanics. Cambridge Lecture Notes in Physics* (Cambridge University Press, Cambridge, 1999). https://doi.org/10.1017/CBO9780511628870.008.
22 Deyle ER, Sugihara G, Generalized theorems for nonlinear state space reconstruction, *PLoS One* **6**, e18295 (2011). https://doi.org/10.1371/journal.pone.0018295.
23 Kennel MB, Brown R, Abarbanel HDI, Determining embedding dimension for phase-space reconstruction using a geometrical construction, *Phys. Rev. A* **45**, 3403 (1992). https://doi.org/10.1103/PhysRevA.45.3403.
24 Abarbanel HDI, *Analysis of observed chaotic data* (Springer, New York, NY, 1996). https://doi.org/10.1007/978-1-4612-0763-4.